Int. J. Solids Structures Vol. 28, No. 5, pp. 533–548, 1991
Printed in Great Britain.

0020–7683/91 $3.00 + .00

DYNAMIC RESPONSE OF A LAYERED HALF-SPACE WITH INTERFACIAL CRACKS

M. BOUDEN and S. K. DATTA
Department of Mechanical Engineering and CIRES, University of Colorado, Boulder, CO 80309-0427, U.S.A.

and

A. H. SHAH
Department of Civil Engineering, University of Manitoba, Winnipeg, Canada R3T 2N2

(*Received* 20 *June* 1990; *in revised form* 19 *August* 1990)

Abstract—The scattering of elastic waves by interfacial cracks in a layered medium is investigated in this paper. A hybrid numerical method is employed to obtain the solution. This method combines the finite element equations and the Green's function boundary integral representation. Numerical results are presented for the crack-opening displacements (CODs) and the Mode I and Mode II stress-intensity factors (SIFs) as functions of nondimensional frequency when normal and tangential time-harmonic line loads are applied to the free surface of the layered medium.

1. INTRODUCTION

In the past 20 years, corrosion-resistant coating technology has received a lot of attention from a multidisciplinary engineering and scientific community for its wide applications. The selection of the coating material, its thickness and the number of coats are usually based on the nature and the degree of aggressiveness of the environment the coated structure will be exposed to. Also, coatings have to be compatible with the base material (substrate) to assure a good bonding. In the steel industry, the most commonly-used processes for applying metal coatings are: hotdipping, electrodeposition, spraying, diffusion and cladding (Suziki, 1989). In all of these processes, it is not unusual to produce a coating with defects, such as cracks, debonding or discontinuities. Moreover, these defects can also occur *in situ* due to fatigue or unusual stress levels applied to the material. The presence of these defects makes the structure vulnerable to failure due to the propagation or growth of these defects. In this paper we examine dynamic loading effects on the crack-opening displacements (CODs) and the stress-intensity factors (SIFs).

Among the works reported during the last decade that deal with scattering by interface cracks is that of Neerhoff (1979), who investigated the diffraction of incident bulk SH and Love waves by a crack of finite width at the interface of a layered medium. He solved the antiplane problem employing the integral equation method. Keer *et al.* (1984) studied the resonance phenomena for a crack near the free surface of a homogeneous half-space. The plane strain problelm was solved by deriving a system of coupled singular integral equations. These integral equations were solved numerically for incident waves generated by uniform tension and shear applied to the free surface. The work done by Yang and Bogy (1985) is the most relevant to our work. They considered a plane strain problem of a layered half-space with a single interfacial crack. The method of solution was similar to that of Neerhoff (1979) for the antiplane problem. It leads to a set of coupled singular integral equations. After discretization of the crack surfaces, these integrals are approximated by an algebraic system of equations that are solved numerically. In a two-part paper, Gracewski and Bogy (1986a,b) applied the same method to investigate the scattering by a crack at the interface of a single-layered medium loaded by an invicid fluid. In the first paper the incident field was generated by a uniform normal and shear traction applied at the liquid–layer interface. Plane waves and bounded beams with a Gaussian profile incident from the fluid side were considered in the second part. The transient response of an interface crack in a two-lalyered plate subject to an antiplane stress field was studied by Kundu (1986). He also employed

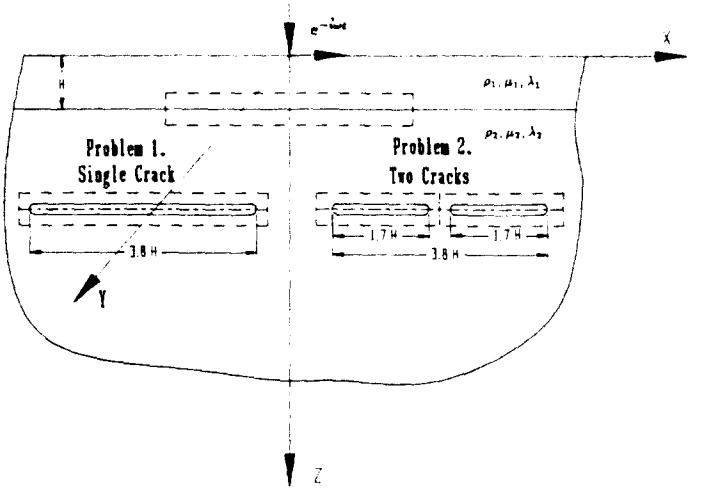

Fig. 1. Layered half-space with two configurations of interfacial cracks.

the integral equation method proposed by Neerhoff. Kundu and Hassan ((1987) solved the same problem for a layered plate of finite length, by discretizing the whole domain with finite elements. First the discretized equation of motion was solved in the frequency domain, then a fast Fourier transform (FFT) technique was used to obtain the time response. More recently, the interaction between two cracks at the interface of a layered isotropic and anisotropic medium under antiplane loading was studied by Kundu (1987) and Karim and Kundu (1988).

In this paper we present a different method for studying the dynamic response of a layered half-space with interfacial cracks due to in-plane surface line loadings. Two problems are investigated using this method, a single long interfacial crack and two smaller cracks separated by a short distance. The sum of the lengths of the two cracks and the separation distance is equal to the length of the single crack (see Fig. 1). The motivation for this particular choice comes from the need to understand the differences in the dynamic response of a fully-open and a slightly-closed crack. The method of solution used here was suggested by Zienkiewicz (1977), and has been applied by Shah *et al.* (1982) for the diffraction of SH waves in a half-space. Franssens and Lagasse (1984) used a similar technique to study the two-dimensional scattering of both SH and P-SV waves by a cylindrical obstacle in a layered medium. The most recent work by Khair *et al.* (1989) is a generalization to three-dimensional amplification of seismic waves by arbitrarily-shaped alluvial valleys embedded in a homogeneous half-space.

This method combines the finite element technique with the boundary integral representation on the boundary of the finite element region to solve for the scattered field. The overlapping of the two regions, which will be discussed in the next section, permits the evaluation of the integrals for source and observation points on two different contours. This avoids the singularities associated with the Green's functions when the source and receiver coincide. The advantage of this method resides in the fact that once the Green's functions are obtained for a given frequency, the scattering due to any irregularity that fits inside the finite element region can be determined. Thus this method differs fundamentally from that employed in the earlier works on interface cracks cited above. Here, instead of using the integral representation over the crack surface, the exterior solution is written as an integral over a surface away from the crack (or scatterer). This allows one to solve for multiple cracks without changing the exterior representation. In the next section an outline of the method is given.

2. FORMULATION

2.1. *Statement of the problem*

The problem considered here is a single layer bonded to a half-space as illustrated in Fig. 1. The layer and half-space are made of linearly elastic, isotropic, homogeneous

materials. When necessary a subscript or superscript (1, 2) is used to describe properties related to the layer and substrate, respectively, e.g. ρ_1, μ_1, λ_1 represent the mass densitiy and the Lamé's constants of the layer. In this paper the dynamic response due to time-harmonic line loads is investigated. In the first problem we consider a large crack of length $3.8H$ located at the interface of the single-layered structure. The second problem consists of two smaller cracks of equal lengths $1.7H$ separated by a distance $D = 0.4\ H$. Here H stands for the layer thickness.

Let u_i be the displacement component in the ith direction in the Cartesian coordinate system shown and τ_{ij} the stress tensor having time-harmonic behavior of the form $e^{-i\omega t}$. The equation of motion in the frequency domain is written as

$$\tau_{ij,j} + \rho\omega^2 u_i = -f_i \quad (i, j = 1, 2, 3) \tag{1}$$

where ρ is the mass density, f_i the body force per unit volume and ω the circular frequency.

The total fields generated by the interaction of the free field with the cracked medium can be expressed as

$$u_i = u_i^s + u_i^f; \quad \tau_{ij} = \tau_{ij}^s + \tau_{ij}^f \tag{2}$$

where the symbols carrying the superscripts s and f are associated with the scattered and free fields, respectively.

It is assumed that the upper surface of the layered medium is traction free and the bonding between the layer and the substrate is perfect except at the cracked regions (cracks or delamination). The crack surfaces are assumed to be traction free. For both problems mentioned above, the boundary and continuity conditions are

$$\tau_{xz}^{(1)} = \tau_{yz}^{(1)} = \tau_{zz}^{(1)} = 0; \quad z = 0; \quad -\infty < x < \infty. \tag{3}$$

Problem 1. Single crack

$$u^{(1)} = u^{(2)}, \quad v^{(1)} = v^{(2)}, \quad w^{(1)} = w^{(2)}; \quad z = H; \quad |x| > 1.9H \tag{4}$$

$$\tau_{xz}^{(1)} = \tau_{xz}^{(2)}, \quad \tau_{yz}^{(1)} = \tau_{yz}^{(2)}, \quad \tau_{zz}^{(1)} = \tau_{zz}^{(2)}; \quad z = H; \quad |x| > 1.9H \tag{5}$$

$$\tau_{xz}^{(1)} = \tau_{yz}^{(1)} = \tau_{zz}^{(1)} = 0; \quad z = H; \quad |x| < 1.9H \tag{6}$$

$$\tau_{xz}^{(2)} = \tau_{yz}^{(2)} = \tau_{zz}^{(2)} = 0; \quad z = H; \quad |x| < 1.9H \tag{7}$$

Problem 2. Two cracks

$$u^{(1)} = u^{(2)}, \quad v^{(1)} = v^{(2)}, \quad w^{(1)} = w^{(2)}; \quad z = H; \quad |x| < 0.2H \text{ and } |x| > 1.9H \tag{8}$$

$$\tau_{xz}^{(1)} = \tau_{xz}^{(2)}, \quad \tau_{yz}^{(1)} = \tau_{yz}^{(2)}, \quad \tau_{zz}^{(1)} = \tau_{zz}^{(2)}; \quad z = H; \quad |x| < 0.2H \text{ and } |x| > 1.9H \tag{9}$$

$$\tau_{xz}^{(1)} = \tau_{yz}^{(1)} = \tau_{zz}^{(1)} = 0; \quad z = H; \quad -1.9H < x < -0.2H \text{ and } 0.2H < x < 1.9H \tag{10}$$

$$\tau_{xz}^{(2)} = \tau_{yz}^{(2)} = \tau_{zz}^{(2)} = 0; \quad z = H; \quad -1.9H < x < -0.2H \text{ and } 0.2H < x < 1.9H \tag{11}$$

Moreover, both fields must satisfy the elastic radiation conditions at infinity. For the general three-dimensional formulation of this problem, we will consider the dependence of the displacement on the y-coordinate to be taken as

$$u_i(x, y, z) = u_i(x, z)\, e^{i\xi y}. \tag{12}$$

This represents a propagating wave in the y-direction with wavelength $2\pi/\xi$ and amplitude varying with x and z. This allows us to consider incident waves that are propagating at an

arbitrary angle to the axis of the crack(s). The method of solution will be discussed in the following sections.

2.2. *Description of the method*

The method of solution used here combines the Green's function boundary integral representation with the finite element equations. A simple fictitious contour B around the scatterer is introduced as shown in Fig. 2. We define the interior region, R_1, to be bounded by B. This region is then discretized with finite elements having $N = N_1 + N_B$ number of nodes, N_1 being the number of nodes interior to B and N_B the number of nodes on B.

As described above, the domain R_1 is divided into finite elements. Let the element domain and the boundary be denoted by $\Omega^{(e)}$ and $\Gamma^{(e)}$, respectively. The displacement field is written in the usual way in terms of the shape functions and the nodal displacements in matrix form as follows:

$$\{\mathbf{u}\} = \begin{Bmatrix} u \\ v \\ w \end{Bmatrix} = \begin{bmatrix} \phi_1 & 0 & 0 & \dots & \phi_n & 0 & 0 \\ 0 & \phi_1 & 0 & \dots & 0 & \phi_n & 0 \\ 0 & 0 & \phi_1 & \dots & 0 & 0 & \phi_n \end{bmatrix} \begin{Bmatrix} u_1 \\ v_1 \\ w_1 \\ \vdots \\ u_n \\ v_n \\ w_n \end{Bmatrix}$$

$$= [\mathbf{\Phi}]\{\mathbf{u}^e\}, \tag{13}$$

in which n denotes the number of nodes per element and the superscript (e) is the element identifier. By using the strain displacement relation we get

$$\{\varepsilon\} = [\mathbf{D}][\mathbf{\Phi}]\{\mathbf{u}^e\} = [\mathbf{B}]\{\mathbf{u}^e\} \tag{14}$$

where $\boldsymbol{\varepsilon} = \{\varepsilon_{xx}, \varepsilon_{yy}, \varepsilon_{zz}, \varepsilon_{yz}, \varepsilon_{xz}, \varepsilon_{xy}\}^t$ and the derivative operator $\mathbf{D}$ is

$$\mathbf{D} = \begin{bmatrix} \dfrac{\partial}{\partial x} & 0 & 0 \\ 0 & i\xi & 0 \\ 0 & 0 & \dfrac{\partial}{\partial z} \\ 0 & \dfrac{\partial}{\partial z} & i\xi \\ \dfrac{\partial}{\partial z} & 0 & \dfrac{\partial}{\partial x} \\ i\xi & \dfrac{\partial}{\partial x} & 0 \end{bmatrix} \tag{15}$$

the superscript t denotes transpose.

The stresses are related to the strains via the constitutive law and may be written in matrix form as

$$\{\tau\} = [\mathbf{C}]\{\varepsilon\} \tag{16}$$

where C is the (6×6) symmetric stiffness matrix. For an isotropic material, all the entries of C are in terms of Lamé's constants λ and μ.

The total energy associated with each element (e) is to be taken as

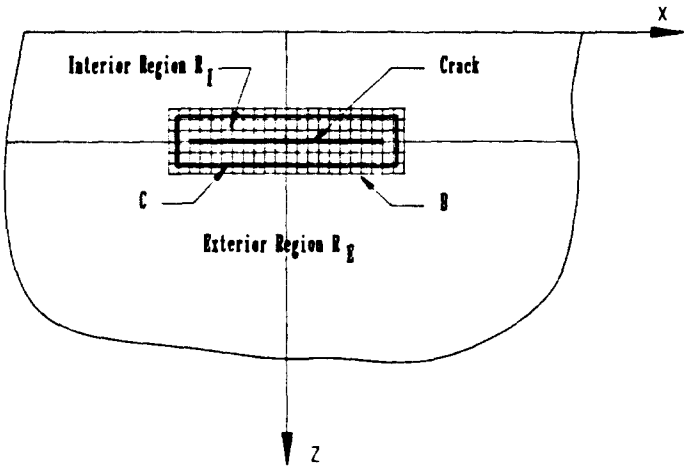

Fig. 2. Contour and regions definition.

$$E^{(e)} = U^{(e)} + \mathscr{K}^{(e)} - W^{(e)} \tag{17}$$

where $U^{(e)}$ and $\mathscr{K}^{(e)}$ are the strain and kinetic energies, respectively, and $W^{(e)}$ is the surface traction work potential; these are defined as

$$U^{(e)} = \frac{1}{2}\int_{\Omega^{(e)}} \{\tau\}^t\{\varepsilon\}^* \, dx\, dz \tag{18}$$

$$\mathscr{K}^{(e)} = -\frac{1}{2}\int_{\Omega^{(e)}} \rho\omega^2\{\mathbf{u}\}^t\{\mathbf{u}\}^* \, dx\, dz \tag{19}$$

$$W^{(e)} = \frac{1}{2}\oint_{\Gamma^{(e)}} (\{\mathbf{u}\}^t\{\mathbf{t}\}^* + \{\mathbf{t}\}^t\{\mathbf{u}\}^*)\, d\Gamma. \tag{20}$$

Here $\{\mathbf{t}\}$ is the traction vector on the boundary and $\{\ \}^*$ represents the complex conjugate of the vector expressions. The integration in the y-direction is carried out over one wavelength and the above expressions represent the energies per wavelength in the same direction.

By setting the first variation of the total energy, δE, to zero one may get the elemental equations of motion written in the following form

$$\mathbf{S}^{(e)}\mathbf{u}^{(e)} = \mathbf{p}^{(e)} \tag{21}$$

where $\mathbf{S}^{(e)}$ is called the elemental impedance matrix and $\mathbf{p}^{(e)}$ is the consistent nodal force vector. These are defined as

$$\mathbf{S}^{(e)} = \int_{\Omega^{(e)}} ([\mathbf{B}^*]^t[\mathbf{C}][\mathbf{B}] - \rho\omega^2[\mathbf{\Phi}]^t[\mathbf{\Phi}])\, dx\, dz \tag{22}$$

and

$$\mathbf{p}^{(e)} = \oint_{\Gamma^{(e)}} \{\mathbf{t}\}^t[\mathbf{\Phi}]\, d\Gamma. \tag{23}$$

The elemental impedance matrices and load vectors are computed and assembled into a global impedance matrix and load vector. The total number of nodes in region R_I is composed of N_B nodes lying on the boundary B and N_I nodes inside. The global equations of motion are partitioned in such a way that the inside nodal displacements appear at the

top and the boundary ones at the bottom. Therefore the discretized equations of motion over the region R_1 become

$$\begin{bmatrix} S_{II} & S_{IB} \\ S_{BI} & S_{BB} \end{bmatrix} \begin{Bmatrix} U_I \\ U_B \end{Bmatrix} = \begin{Bmatrix} 0 \\ P_B \end{Bmatrix}. \tag{24}$$

For solution purposes, only a relationship between the inside nodal displacements and the boundary ones is needed and this is given by

$$\{U_I\} = -[S_{II}]^{-1}[S_{IB}]\{U_B\}. \tag{25}$$

The boundary integral representation is derived from the elastodynamic reciprocity theorem (Achenbach, 1973), written in the following form:

$$\int_A (\{\mathbf{g}\}^{\mathrm{T}}\{\mathbf{u}\} - \{\mathbf{f}\}^{\mathrm{T}}\{\mathbf{v}\})\,\mathrm{d}A = \oint_C (\{\mathbf{t}\}^{\mathrm{T}}\{\mathbf{v}\} - \{\mathbf{q}\}^{\mathrm{T}}\{\mathbf{u}\})\,\mathrm{d}C \tag{26}$$

where $\mathbf{u}$, $\mathbf{t}$ are the displacement and traction on the boundary C of the region A associated with the body force $\mathbf{f}$, and $\mathbf{v}$, $\mathbf{q}$ are those associated with $\mathbf{g}$. We shall denote the region exterior to C as R_E. Note that the region between the contours B and C is common to R_E and R_I. We will apply the above theroem to the region R_E, with the first field as the scattered field and the second one as the line source Green's function solution. For this purpose we define the Green's function and the scattered fields as solutions to the following equations

$$\Sigma_{kij,j} + \rho\omega^2 G_{ki} = -\delta_{ki}\delta(x-x')\delta(z-z')\,\mathrm{e}^{\mathrm{i}(\omega t + \zeta x)} \tag{27}$$

and

$$\tau^{\mathrm{s}}_{ij,j} + \rho\omega^2 u^{\mathrm{s}}_i = 0. \tag{28}$$

In the above equations, i stands for the displacement direction and k for the force direction. The Green's function solution for a layered medium was derived by Bouden (1990).

After direct substitution of these two fields into eqn (26), we get

$$u^{\mathrm{s}}_k(x', z') = \oint_C (\tau^{\mathrm{s}}_{ij} G_{ki} - \Sigma_{kij} u^{\mathrm{s}}_i) n_j\,\mathrm{d}C. \tag{29}$$

The contour integration is carried out in a clockwise manner.

Applying the elastodynamic reciprocity theorem [eqn (26)] to the region interior to C with the two fields as the Green's solution and the free field with no forcing terms we get

$$\oint_C (\tau^{\mathrm{f}}_{ij} G_{ki} - \Sigma_{kij} u^{\mathrm{f}}_i)(-n_j)\,\mathrm{d}C = 0. \tag{30}$$

The above integral is evaluated in a counterclockwise manner. Combining eqns (29) and (30), one obtains the integral representation of the total displacement at any point in the region R_E as

$$u_k(x', z') = u^{\mathrm{f}}_k(x', z') + \oint_C (\tau_{ij} G_{ki} - \Sigma_{kij} u_i) n_j\,\mathrm{d}C. \tag{31}$$

Noe eqn (31) is evaluated for points (x', z') coinciding with the nodes on the boundary B. This leads to an equation connecting the displacements at the nodes on B to those at the nodes on C in the form

$$\{U_B\} = \{U_B^f\} + \left[\oint_C ([\mathbf{G}][\mathbf{C}][\mathbf{B}_C] - [\mathbf{\Phi}_C]^t[\Sigma])\{\mathbf{n}\}\,dC\right]\{U_C\} + \left[\oint_C ([\mathbf{G}][\mathbf{C}][\mathbf{B}_B] - [\mathbf{\Phi}_B]^t[\Sigma])\{\mathbf{n}\}\,dC\right]\{U_B\} \quad (32)$$

where $[\mathbf{B}_C] = [\mathbf{D}][\mathbf{\Phi}_C]$ and $[\mathbf{B}_B] = [\mathbf{D}][\mathbf{\Phi}_B]$.

Using eqn (32) and completing U_C with the remaining inside nodal displacements, yields

$$\{U_B\} = [A_{BI}]\{U_I\} + [A_{BB}]\{U_B\} + \{U_B^f\}, \quad (33)$$

where $[A_{BI}]$ is a $(3N_B \times 3N_I)$ and $[A_{BB}]$ is a $(3N_B \times 3N_B)$ complex matrix. Substituting eqn (25) into eqn (33) and solving for $\{U_B\}$, we get

$$\{U_B\} = \{[I] + [A_{BI}][S_{II}]^{-1}[S_{IB}] - [A_{BB}]\}^{-1}\{U_B^f\}. \quad (34)$$

The inside nodal displacements can then be determined by using eqn (25). The displacement at any point in the region R_E can be found by applying eqn (31).

3. NUMERICAL RESULTS AND DISCUSSION

Numerical results were obtained for a nickel coating layer over an iron substrate. Single-layer coatings are usually of the order of microns topping base materials of several millimeters. This contrast in thickness justifies the single-layered half-space model. In our analysis, all the material and geometric parameters were nondimensionalized. Lengths were normalized with respect to the layer thickness H. The material constants and densities were normalized with respect to the layer rigidity and density, respectively. Then, the layer thickness, rigidity and density were set to unity. Finally, all the wavenumbers were normalized with respect to the layer shear wavenumber k_{21}.

The material properties of nickel and iron are listed in Table 1. Here σ_i is Poisson's ratio and C_{1i}, C_{2i} and C_{Ri} are the longitudinal, shear and Rayleigh wave velocities, respectively. This case can be classified as a "loading" case according to Farnell and Adler (1972), because the layer shear velocity is less than the half-space shear velocity (i.e. $C_{21} < C_{22}$). For this case, multiple Rayleigh-like guided wave modes occur. Figure 3 shows the dispersion behavior of these guided modes. The velocities of these modes, which are frequency dependent, are higher than the layer Rayleigh velocity C_{R1}. The numerical integration of the semi-infinite wavenumber-type of integrals that arise in the evaluation of the Green's displacements and their associated stresses is discussed by Xu and Mal (1987) and Bouden (1990). We define the nondimensional frequency ε as $k_{21}H$. Two problems are considered here. Firstly, a single Griffith crack at the interface of this layered material. The length of the crack is $a = 3.8H$. Secondly, two identical cracks of length $1.7H$ separated by a distance $D = 0.4H$ between their inner tips are considered.

The incident field is caused by a time-harmonic line load applied at the origin of the coordinate system (Fig. 1). Both normal and tangential loads are considered.

The internal region R_I was discretized into finite elements. The mesh for the single crack had 316 elements and 506 nodes. For the two-crack mesh, 356 elements and 557 nodes were used. Regular isoparametric elements were used everywhere except at the crack

Table 1. Material properties

Material (i)	σ_i	ρ_i (g cm^{-3})	C_{1i} (km s^{-1})	C_{2i} (km s^{-1})	C_{Ri} (km s^{-1})
Nickel	0.31	8.8	5.24	2.75	2.55
Iron	0.28	7.7	5.72	3.16	2.92

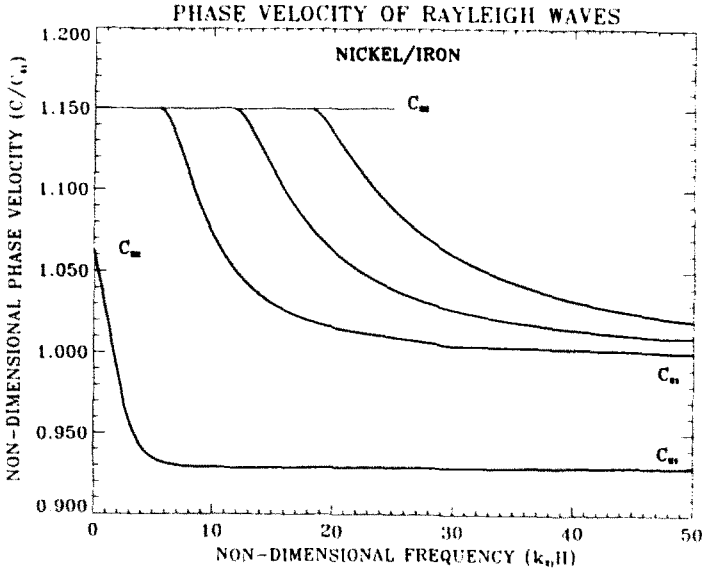

Fig. 3. Phase velocity for the first four Rayleigh modes for a nickel layer over an iron substrate.

tips, where eight six-node triangular quarter-point elements were used. Barsoum (1976) showed that these singular elements can model crack-tip singularity in a homogeneous medium. However, it has been show that the stress singularity at the tip of an interfacial crack is oscillatory if the crack faces are smooth and perfect bonding is assumed outside the crack tips (see Williams, 1959 and Bogy, 1971). This well-known oscillating singularity satisfies the following equation

$$\beta^2 \sin^2(\alpha\pi) + \cos^2(\alpha\pi) = 0$$

which has the solution

$$\alpha = \tfrac{1}{2} \pm \frac{\hat{\imath}}{2\pi} \ln\left(\frac{1+\beta}{1-\beta}\right)$$
$$= \tfrac{1}{2} \pm \hat{\imath}\eta \tag{35}$$

where

$$\beta = \frac{\mu_2(1-2\sigma_1) - \mu_1(1-2\sigma_2)}{2\mu_2(1-\sigma_1) + 2\mu_1(1-\sigma_2)}.$$

For the material combination used here, $\beta = 0$ and $\alpha = \frac{1}{2}$. Thus the singularity is identical to the case of a homogeneous material.

The finite element discretization and the numerical evaluation of the contour integral are the only sources of inaccuracy in this method. The size of the elements and number of Gauss points per element were varied to keep the relative error less than 5%. It was found that 10 elements per wavelength is the minimum to capture the physics of the problem and also three Gauss points per elements for the contour integration are enough for the desired accuracy. A comparison with published results can be found in Bouden (1990).

3.1. *Crack-opening displacements*

Crack-opening and sliding displacements (CODs) were computed at different non-dimensional frequencies. Considering the geometric and loading symmetry, only the CODs

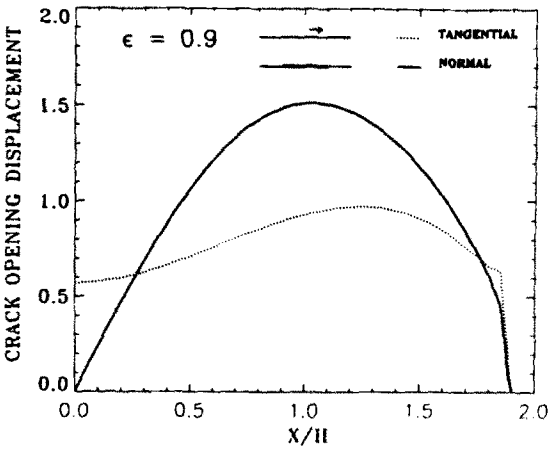

Fig. 4. Crack opening and sliding for the right half of the single crack. This result is for a tangential time-harmonic line load with a nondimensional frequency $\varepsilon = 0.9$.

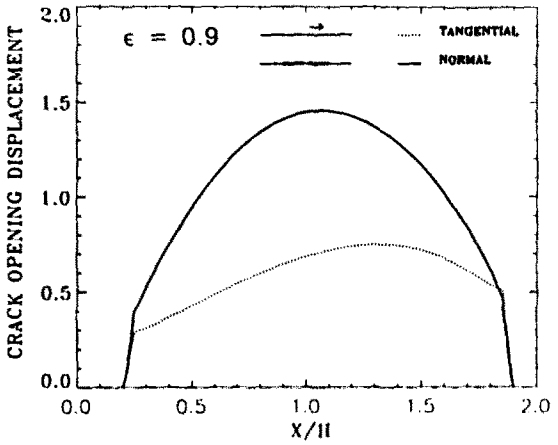

Fig. 5. Crack opening and sliding for the right crack. This result is for a tangential time-harmonic line load with a nondimensional frequency $\varepsilon = 0.9$.

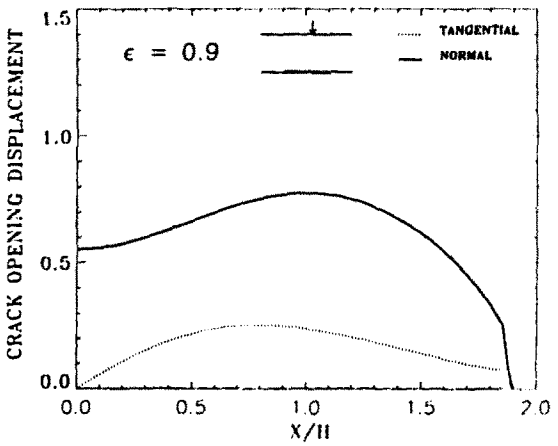

Fig. 6. Crack opening and sliding for the right half of the single crack. This result is for a normal time-harmonic line load with a nondimensional frequency $\varepsilon = 0.9$.

on the right half are shown in Figs 4–7 for $\varepsilon = 0.9$. The dotted line represents the in-plane sliding of the crack surfaces, while the solid line represents the opening of the crack. The arrow on top of the layer is the force direction. Figures 4 and 5 show the CODs for the single and double crack configurations. It is interesting to note from these figures that

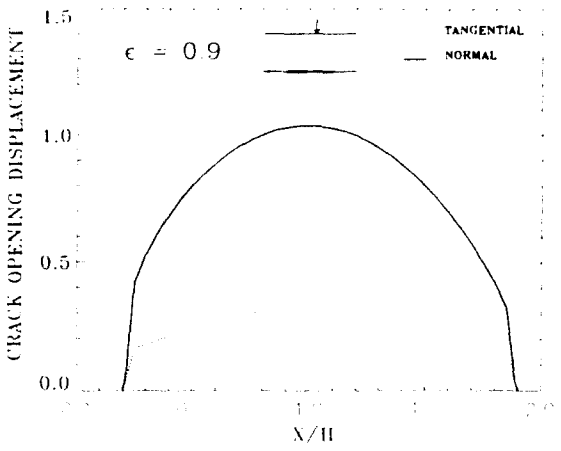

Fig. 7. Crack opening and sliding for the right crack. This result is for a normal time-harmonic line load with a nondimensional frequency $\varepsilon = 0.9$.

the crack-opening displacements have the same shapes for $X/H > 0.2$. Also, the normal displacements in both cases are nearly the same in this region. This is a rather surprising result. Note that the normal displacement is larger than the sliding displacement over most of the crack surface for the single crack and over the entire crack surfaces for double cracks. It was found that as the frequenncy was increased the CODs decreased. Also, the sliding displacement's amplitude became larger than the normal displacement's.

Figures 6 and 7 show the results for a normal line load. The CODs for the single and double cracks behave quite differently now. It is found from Figs 6 and 7 that the normal COD is larger than the tangential one. Furthermore, the CODs are larger for the double cracks than for the single crack. At high frequencies it was found that the shapes of the CODs become oscillatory and are of similar shapes for both crack configurations.

3.2. *Stress-intensity factors*

The stress-intensity factors K_1 and K_2 can be extracted from the finite element solution by identification of the coefficients of the singular terms in the analytical expressions for the displacement fields in the vicinity of the crack tip with the interpolated expressions from the six-noded triangular quarter-point elements.

The analytical expressions for the displacement fields in the vicinity of a crack tip along the bond line of two half-spaces of different materials shown in Fig. 8 can be derived in the same manner as for the homogeneous case. The biharmonic Airy stress function solution to this plane problem can be expressed in terms of the complex Goursat functions of the complex variable $z = x + iy$ as follows:

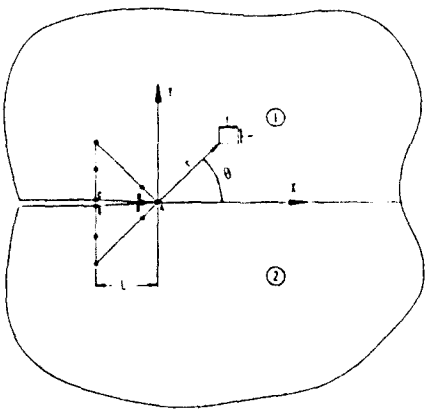

Fig. 8. Geometry of an interface crack between bonded dissimilar half-spaces and crack-tip elements.

$$U_i(z) = \mathrm{Re}\,[\bar{z}\phi_i(z) + \chi_i(z)]; \tag{36}$$

here i takes the values 1 and 2 for $y > 0$ and $y < 0$, respectively.

For this problem, the general forms of the Goursat functions were given by Sih and Rice (1964) as

$$\phi_1(z) = 2z^{-1/2-i\eta} \sum_{n=1}^{\infty} [(n+\tfrac{1}{2}) - i\eta]\bar{B}^{(n)} z^n \tag{37}$$

$$\chi_1(z) = 2e^{2\pi\eta} z^{-1/2+i\eta} \sum_{n=1}^{\infty} B^{(n)} z^n - 2z^{-1/2-i\eta} \sum_{n=1}^{\infty} [(n-\tfrac{1}{2}) - i\eta]\bar{B}^{(n)} z^n \tag{38}$$

for the region $y > 0$ and

$$\phi_2(z) = 2e^{2\pi\eta} z^{-1/2-i\eta} \sum_{n=1}^{\infty} [(n+\tfrac{1}{2}) - i\eta]\bar{B}^{(n)} z^n \tag{39}$$

$$\chi_2(z) = 2z^{-1/2+i\eta} \sum_{n=1}^{\infty} B^{(n)} z^n - 2e^{2\pi\eta} z^{-1/2-i\eta} \sum_{n=1}^{\infty} [(n-\tfrac{1}{2}) - i\eta]\bar{B}^{(n)} z^n \tag{40}$$

for the region $y < 0$. In eqns (37) through (40), η is the bielastic constant given by eqn (35). It can be shown after some algebra that the crack-tip displacements and stress-intensity factors satisfy the following relations for the case $\eta = 0$:

$$u_1 = \frac{1}{4\mu_1}\sqrt{\frac{r}{2}}\left\{k_1\left[(2\kappa_1 - 1)\cos\frac{\theta}{2} - \cos\frac{3\theta}{2}\right] + k_2\left[(2\kappa_1 + 3)\sin\frac{\theta}{2} + \sin\frac{3\theta}{2}\right]\right\} \tag{41}$$

$$v_1 = \frac{1}{4\mu_1}\sqrt{\frac{r}{2}}\left\{k_1\left[(2\kappa_1 + 1)\sin\frac{\theta}{2} - \sin\frac{3\theta}{2}\right] - k_2\left[(2\kappa_1 - 3)\cos\frac{\theta}{2} + \cos\frac{3\theta}{2}\right]\right\} \tag{42}$$

$$u_2 = \frac{1}{4\mu_2}\sqrt{\frac{r}{2}}\left\{k_1\left[(2\kappa_2 - 1)\cos\frac{\theta}{2} - \cos\frac{3\theta}{2}\right] + k_2\left[(2\kappa_2 + 3)\sin\frac{\theta}{2} + \sin\frac{3\theta}{2}\right]\right\} \tag{43}$$

$$v_2 = \frac{1}{4\mu_2}\sqrt{\frac{r}{2}}\left\{k_1\left[(2\kappa_2 + 1)\sin\frac{\theta}{2} - \sin\frac{3\theta}{2}\right] - k_2\left[(2\kappa_2 - 3)\cos\frac{\theta}{2} + \cos\frac{3\theta}{2}\right]\right\}; \tag{44}$$

here $\kappa_i = 3 - 4\sigma_i$ for this plane strain case. Note that these expressions are identical with the homogeneous solution derived by Williams (1957).

The collapsed quadrilateral quarter-point element contains terms in the interpolated displacement fields proportional to the square root of the radial distance r emanating from the crack tip. For instance, the displacement field components along the edges containing the nodes A, B, C and A, D, E shown in Fig. 8 are given by Owen and Fawkes (1983), i.e.

$$u_1 = u_A + (4u_B - u_C - 3u_A)\sqrt{\frac{r}{L}} + (2u_C + 2u_A - 4u_B)\frac{r}{L} \tag{45}$$

$$v_1 = v_A + (4v_B - v_C - 3v_A)\sqrt{\frac{r}{L}} + (2v_C + 2v_A - 4v_B)\frac{r}{L} \tag{46}$$

$$u_2 = u_A + (4u_D - u_E - 3u_A)\sqrt{\frac{r}{L}} + (2u_E + 2u_A - 4u_D)\frac{r}{L} \tag{47}$$

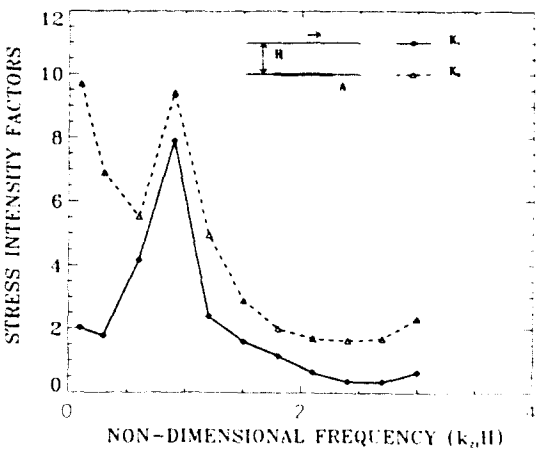

Fig. 9. Mode I and Mode II stress-intensity factors as a function of nondimensional frequency at crack tip A of the single crack for a tangential load.

$$v_2 = v_A + (4v_D - v_E - 3v_A)\sqrt{\frac{r}{L}} + (2v_E + 2v_A - 4v_D)\frac{r}{L} \tag{48}$$

The Mode I and Mode II stress-intensity factors presented in Figs 9–14 are obtained by equating the coefficients of $\sqrt{r}$ in eqns (41)–(44) and (45)–(48). We have

$$K_1 = |k_1| = \left| \frac{2\mu_1}{\kappa_1 + 1}\sqrt{\frac{2}{L}}(4v_B - v_C - 3v_A) \right| \tag{49}$$

or

$$K_1 = |k_1| = \left| -\frac{2\mu_2}{\kappa_2 + 1}\sqrt{\frac{2}{L}}(4v_D - v_E - 3v_A) \right| \tag{50}$$

and

$$K_2 = |k_2| = \left| \frac{2\mu_1}{\kappa_1 + 1}\sqrt{\frac{2}{L}}(4u_B - u_C - 3u_A) \right| \tag{51}$$

or

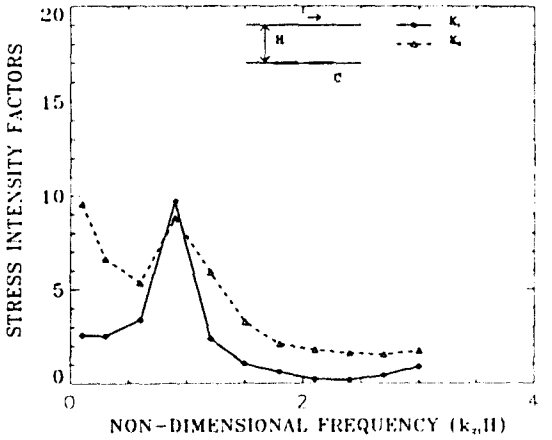

Fig. 10. Mode I and Mode II stress-intensity factors as a function of nondimensional frequency at crack tip C of the single crack for a tangential load.

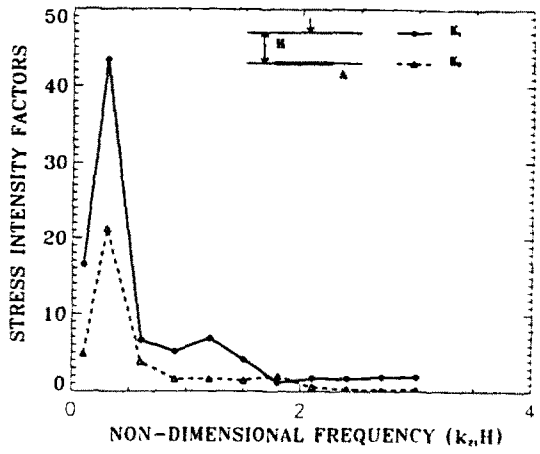

Fig. 11. Mode I and Mode II stress-intensity factors as a function of nondimensional frequency at crack tip A of the single crack for a normal load.

$$K_2 = |k_2| = \left| -\frac{2\mu_2}{\kappa_2+1}\sqrt{\frac{2}{L}}(4u_D - u_E - 3u_A) \right|. \tag{52}$$

The numerical values of the stress-intensity factors presented here are the average of eqns (49) and (50) for mode I and eqns (51) and (52) for mode II.

Figure 9 shows K_1 and K_2 for crack tip A versus the nondimensional frequency $\varepsilon = k_{21}H$ for a horizontal time-harmonic line load, which is applied on the surface of the layer. K_1 and K_2 for the double-crack case at tip C are depicted by Fig. 10. It is observed that K_1 and K_2 in both cases start at the same values for low frequencies, then they decrease (K_2 decreasing more rapidly than K_1) and then increase to a peak at about $\varepsilon \approx 0.9$. Beyond this frequency, they gradually decrease. Note that K_2 is dominant, as would be anticipated from the nature of the loading. For the double cracks, however, both K_1 and K_2 reach nearly the same peak. Note that in both cases mode I dynamic SIFs are substantially higher than the static values in some ranges of frequencies. On the other hand, the mode II SIFs have somewhat higher static values. Figures 11 and 12 show K_1 and K_2 for a normal loading. In this case the roles are reversed. The opening mode dominates. It is found now that for the single crack K_1 and K_2 increase with frequency reaching sharp peak values at a lower frequency, i.e. $\varepsilon \approx 0.3$. This lowering of the resonance frequency from the shear loading case to the normal case is in agreement with the results obtained by Keer *et al.* (1984) for a horizontal crack buried near the surface of a half-space due to uniform shear and tension loadings. Figure 12 for the double crack shows quite different behavior than for the single

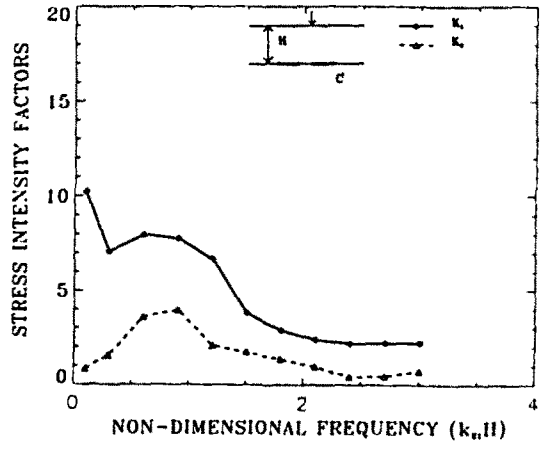

Fig. 12. Mode I and Mode II stress-intensity factors as a function of nondimensional frequency at crack tip C of the right crack for a normal load.

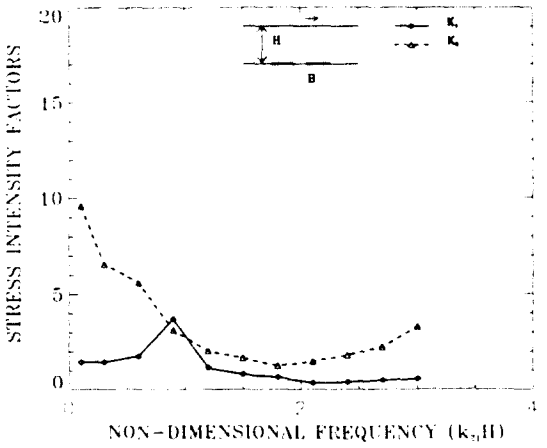

Fig. 13. Mode I and Mode II stress-intensity factors as a function of nondimensional frequency at crack tip B of the right crack for a tangential load.

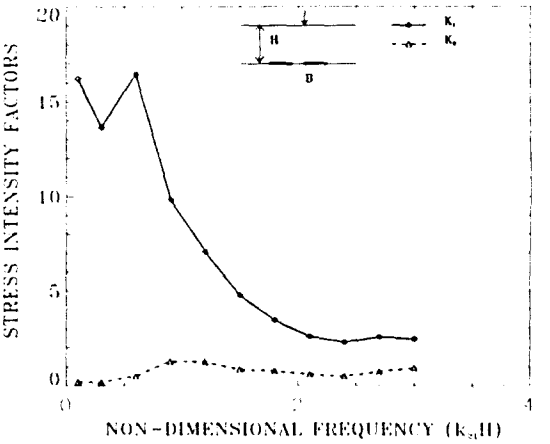

Fig. 14. Mode I and Mode II stress-intensity factors as a function of nondimensional frequency at crack tip B of the right crack for a normal load.

crack. It is seen that for the single crack the dynamic SIFs (both K_1 and K_2) are much higher than the static values at low frequencies. For the double-crack configuration the dynamic K_1 is lower and K_2 is higher than the static values. Finally, K_1 and K_2 at crack tip B for shear and normal loading are depicted by Figs 13 and 14, respectively. For the horizontal loading case, both stress-intensity factors at B are lower than those evaluated at C (Fig. 10). In the case of vertical loading, K_1 at tip B is higher than at tip C for both static and dynamic loadings. Moreover, the dynamic effect is quite large. K_2, on the other hand, is lower at B than at C. It is clear from the dispersion curves depicted in Fig. 3 that the frequency values at which K_1 and K_2 have local maxima do not correspond to a cut-off frequency. However, when the frequencies at these peak values are compared to the natural frequencies of a Timoshenko plate of length $3.8H$ (Table 2) with two different boundary

Table 2. Natural frequencies for a Simply Supported (SS) and Clamped (C) Timoshenko plate and frequency values at peaks of stress-intensity factors

	$\varepsilon = k_2 H$	
Mode	1 (ω_{11})	2 (ω_{21})
SS	0.34	0.40
C	0.76	0.94
Peak	0.3	0.9

conditions (simply supported or clamped), they show a good correlation. For tangential loading the peak occurs at $\varepsilon \simeq 0.9$. This value is bounded by the two natural frequencies of the second mode (ω_{21}), with the lower and upper bounds corresponding to the simply supported (SS) and clamped (C) case, respectively. In the case of normal loading the peak occurs at $\varepsilon \simeq 0.3$. This value is slightly lower than the natural frequency of the first mode (ω_{11}) for the simply-supported case. However, since the frequency increment is 0.3, the accuracy of these peak frequency values is within this increment. It is concluded from these figures that the dynamic effects are quite substantial and, in general, give higher values of K_1 for normal impact at low frequencies. The worst case is a single interfacial crack.

4. CONCLUSION

A combined finite-element and integral representation technique has been presented to analyze scattering of waves by interfacial cracks in a layered half-space. The advantage of the technique is that both single and multiple cracks have been studied simply by changing some of the interior elements. Consequently, the computation of the Green's function is done once and for all by choosing the exterior boundaries B and C appropriately so that all the scatterers are within C. Thus this differs from the integral equation methods that employ representations over the scatterer surface(s). Numerical results showing CODs and SIFs for a single crack and for two cracks due to normal and shear line loads have been presented. It is found that the CODs have similar shapes in both cases at low frequencies, although there are some differences in detail that depend on the frequency. The stress-intensity factors at the outer tips in both cases are found to behave similarly for the horizontal load. However, they behave quite differently for the vertical load. For the vertical load the mode I stress-intensity factor at the inner tips for the double cracks is found to be larger than that at the outer tips. Dynamic stress-intensity factors are found to attain high peak values at certain frequencies, depending on the loading. The loading and boundary conditions at the upper layer surface considered here are quite different from those considered by Gracewski and Bogy (1986a,b), so the results for the single crack considered here cannot be compared with theirs.

Acknowledgements—The work reported here was supported in part by a grant from the Office of Naval Research (No. N00014-86-K-0280). The first author is grateful to the Tunisian government for granting a scholarship for his graduate studies. The numerical computations were carried out on CRAY-XMP/48 at the National Center for Supercomputing Applications at the University of Illinois, Urbana.

REFERENCES

Achenbach, J. D. (1973). *Wave Propagation in Elastic Solids*. North-Holland, London.

Barsoum, R. S. (1976). On the use of isoparametric finite elements in linear fracture mechanics. *Int. J. Numer. Meth. Engng* **10**, 25–37.

Bogy, D. B. (1971). Two edge-bonded elastic wedges of different materials and wedge angles under surface tractions. *ASME J. Appl. Mech.* **38**, 377–386.

Bouden, M. (1990). Wave propagation and scattering in layered media: application to earthquake ground motion and ultrasonic nondestructive evaluation of interfacial cracks. Ph.D. Dissertation, University of Colorado, Boulder.

Farnell, G. W. and Adler, E. L. (1972). *Elastic Wave Propagation in Thin Layers. Physical Acoustics*, Vol. 9, pp. 85–127. Academic Press, New York.

Franssens, G. R. and Lagasse, P. E. (1984). Scattering of elastic waves by a cylindrical obstacle embedded in a multilayered medium. *J. Acoust. Soc. Am.* **76**, 1535–1542.

Gracewski, S. M. and Bogy, D. B. (1986a). Elastic wave scattering from an interface crack in a layered half space submerged in water: Part I: Applied tractions at the liquid–solid interface. *ASME J. Appl. Mech.* **53**, 326–332.

Gracewski, S. M. and Bogy, D. B. (1986b). Elastic wave scattering from an interface crack in a layered half space submerged in water: Part II: Incident plane waves and bounded beams. *ASME J. Appl. Mech.* **53**, 333–338.

Karim, M. R. and Kundu, T. (1988). Transient surface response of layered isotropic and anisotropic half-spaces with interface cracks: SH Case. *Int. J. Fracture* **37**, 245–262.

Keer, L. M., Lin, W. and Achenbach, J. D. (1984). Resonance effects for a crack near a free surface. *ASME J. Appl. Mech.* **51**, 65–70.

Khair, K. R., Datta, S. K. and Shah, A. H. (1989). Amplification of obliquely incident seismic waves by cylindrical alluvial valleys of arbitrary cross sectional shape: Part I. Incident P and SV waves. *Bull. Seism. Soc. Am.* **79**, 610–630.

Kundu, T. (1986). Transient response of an interface crack in a layered plate. *ASME J. Appl. Mech.* **53**, 579–586.

Kundu, T. (1987). The transient response of two cracks at the interface of a layered half-space. *Int. J. Engng Sci.* **25**, 1427–1439.

Kundu, T. and Hassan, T. (1987). A numerical study of the transient behavior of an interfacial crack in a bimaterial plate. *Int. J. Fracture* **35**, 55–69.

Neerhoff, F. L. (1979). Diffraction of Love waves by a stres-free crack of finite width in the plane interface of a layered composite. *Appl. Scientific Res.* **35**, 265–315.

Owen, D. R. J. and Fawkes, A. J. (1983). *Engineering Fracture Mechanics: Numerical Methods and Applications*. Pineridge Press, Swansea.

Shah, A. H., Wong, K. C. and Datta, S. K. (1982). Diffraction of plane SH waves in a half-space. *Int. J. Earthquake Engng Struct. Dyn.* **10**, 519–528.

Sih, G. C. and Rice, J. R. (1964). The bending of plates of dissimilar materials with cracks. *ASME J. Appl. Mech.* **31**, 477–482.

Suziki, I. (1989). *Corrosion-Resistant Coatings Technology*. Marcel Dekker, New York.

Williams, M. L. (1957). On the stress distribution at the base of a stationary crack. *ASME J. Appl. Mech.* **24**, 109–114.

Williams, M. L. (1959). The stresses around a fault or crack in dissimilar media. *Bull. Seism. Soc. Am.* **49**, 199–204.

Xu, P.-C. and Mal, A. K. (1987). Calculation of the inplane Green's functions for a layered viscoelastic solid. *Bull. Seism. Soc. Am.* **77**, 1823–1837.

Yang, H. J. and Bogy, D. B. (1985). Elastic wave scattering from an interface crack in a layered half space. *ASME J. Appl. Mech.* **52**, 42–50.

Zienkiewicz, O. C. (1977). *Finite Element Method*. McGraw-Hill, London.